Available online at www.sciencedirect.com
ScienceDirect
Journal of the European Ceramic Society 30 (2010) 423–428
www.elsevier.com/locate/jeurceramsoc

Preparation and characterization of $Zn^{18}O/Zn^{16}O$ isotope heterostructure thin films

Kenji Matsumoto [a,b,*], Yutaka Adachi [b], Isao Sakaguchi [b], Naoki Ohashi [b,a], Hajime Haneda [b,a]

[a] *Department of Applied Science for Electronics and Materials, Interdisciplinary Graduate School of Engineering Sciences, Kyushu University, 6-1 Kasuga-kouen, Kasuga, Fukuoka 816-8580, Japan*
[b] *National Institute for Materials Science, 1-1 Namiki, Tsukuba, Ibaraki 305-0044, Japan*

Abstract

An oxygen isotope-based heterostructure zinc oxide (ZnO) thin film, $Zn^{16}O/Zn^{18}O/Zn^{16}O$, was made by pulsed laser deposition on an *a*-face sapphire substrate. The isotope-enriched $Zn^{18}O$ layer was made by irradiation of the isotope oxygen radical ($^{18}O^*$). The isotopic ratio in the heterostructure film was analyzed via secondary ion mass spectroscopy (SIMS). The ratio of exchange from ^{16}O to ^{18}O was approximately 70% when the oxygen isotope was irradiated as a radical, while it was approximately 10% when the oxygen isotope was supplied as $^{18}O_2$ gas.
© 2009 Elsevier Ltd. All rights reserved.

Keywords: Films; Defects; ZnO; SIMS

1. Introduction

Zinc oxide (ZnO) is a functional metal oxide useful in many optical and electronic applications due to its unique properties.[1] Recently, it has been shown to offer many possibilities when used in thin film technology, i.e. as a semiconducting,[2] photoconducting,[3] piezoelectric[4,5] and an optical waveguide material.[6,7] In order to improve or modify the properties of thin films, modulation doping or superlattice fabrication is generally carried out.[8,9] These kinds of modifications have been intensely attempted for oxide thin film materials. Ohta et al. created superlattices with $SrTiO_3/SrTi_{0.8}Nb_{0.2}O_3/SrTiO_3$ heterostructures, and obtained a high dimensionless figure of merit ($ZT = S^2\sigma T\kappa^{-1}$), exceeding 2 for a thermoelectric device.[10] A superlattice was also applied to improve the optical properties of thin films of the ZnO system, ZnO/(Zn, Mg).[11]

In these conventional modifications with the superlattice, the periodicity in the layers with the alternative element with the host material elements in the growth direction leads to zone-folding of both the electronic band structures and the phonon dispersion curves, and complicates the understanding of phenomena caused by the structures. In order to clarify the phonon properties, isotope superlattices have been fabricated in semiconductor field. Göbel et al. formed $(^{69}GaX)_n(^{71}GaX)_n$ [X = P or As] and observed Raman spectra changes due to the isotopic superlattice.[12] Morita et al. also fabricated $^{70}Ge_n/^{74}Ge_n$ isotope superlattices,[13] and observed zone-folding of optical phonons due to mass periodicity in the growth direction.

Exotic properties are expected with bulk isotopic modification because of the effects of the presence of the isotope, and Itoh's group is currently studying these issues.[14,15] It is well known that $SrTiO_3$ shows quantum paraelectricity below 4 K.[16] Itoh et al. claimed that ferroelectricity was induced in $SrTiO_3$ by the isotope exchange of ^{18}O for ^{16}O.[14] They also indicated that partially isotope-exchanged $SrTiO_3$ shows a high dielectric constant of ~172,000 in the vicinity of the composition for the quantum limit, whereas unexchanged or fully exchanged $SrTiO_3$ shows lower values.[15] In the case of ZnO, the isotopic mass dependence of the A, B, and C direct excitonic band gaps of ZnO was evaluated at low temperatures.[17] Isotopic disorder broadening was reported in Raman spectra.[18] However, there has been no report on hetero-isotopic thin films in oxide systems thus far. If it can be realized, unique materials can be expected, e.g. the temperature coefficient of delay for "Surface Acoustic Wave (SAW)" and "Bulk Acoustic Resonator (BAR)" devices could be controlled, because acoustic velocity is strongly influenced

* Corresponding author at: Department of Applied Science for Electronics and Materials, Interdisciplinary Graduate School of Engineering Sciences, Kyushu University, 6-1 Kasuga-kouen, Kasuga, Fukuoka 816-8580, Japan.
Tel.: +81 29 860 4665; fax: +81 29 855 1196.
E-mail address: MATSUMOTO.Kenji@nims.go.jp (K. Matsumoto).

0955-2219/$ – see front matter © 2009 Elsevier Ltd. All rights reserved.
doi:10.1016/j.jeurceramsoc.2009.06.023

by the isotopic composition and structure. It is believed that *ZT* (dimensionless figure of merit) for thermoelectric devices should be optimized, because isotopic heterostructures of thin films allow for the ability to control electrical and phonon properties independently, and yield strong anisotropy of phonon properties while maintaining the symmetry of the electrical structure.

We are currently studying the fabrication of isotopic heterostructure thin films with a crystal wurtzite structure. We have previously reported the deposition process for $Ga^{14}N/Ga^{15}N/Ga^{14}N$ isotopic hetero-thin films,[19] wherein thin films were deposited using an MBE method, with Ga metal and N radical as sources. In the present study, we develop a process to deposit hetero-isotopic thin films of $Zn^{16}O/Zn^{18}O/Zn^{16}O$. A pulsed laser deposition (PLD) method was applied for this purpose. The sputtering method, commonly used to deposit ZnO thin films, is disadvantageous, because it would require a massive amount of the isotope ^{18}O, even it could be applied as a gaseous phase. On the contrary, although PLD has a comparatively simple operation, high quality thin films can be obtained, similar to the MBE method. Using an oxygen radical source, the isotopic heterostructure, $Zn^{16}O/Zn^{18}O/Zn^{16}O$, was successfully obtained. ZnO with natural oxygen isotope abundance was used as a target for the PLD process. We also discuss the exchange mechanism between the target oxygen and the introduced oxygen radical.

2. Experimental procedure

The isotopic heterostructured ZnO thin films were grown using the pulsed laser deposition (PLD) method (equipment: Pascal Co., Ltd.).[20] The polycrystalline ZnO target was synthesized by a conventional ceramic method. ZnO powder (5N-grade, Kojundo Chemical Laboratory Co., Ltd.) was compacted into disk-shaped pellets with Ø 20 mm diameter and 5 mm thickness under 20 MPa uniaxial pressure. The pellets were sintered at 1323 K for 2 h in air – a sintered body has a theoretical density of above 99%. The pellets were polished using diamond slurry to a mirror-face. These were used as a PLD target after cleaning with ethanol and acetone using an ultrasonic cleaner. α-Al_2O_3 single crystals with mirror polished *a*-face[21] (Kyocera Co., Ltd.) were used as substrates for the PLD.

The fourth harmonic generation (FHG) of a Nd:YAG laser (Quantel, Brilliant B, $\lambda = 266$ nm) was employed and irradiated at 5 Hz on the ZnO targets. Various growth temperatures for the film were used. The vacuum chamber for the deposition was evacuated to 1.0×10^{-6} Pa base pressure prior to film growth. During the film growth, the distance between the substrate and the target ceramics was maintained at 50 mm, and the pressure of the $^{18}O_2$ (isotopic purity: 99%, Taiyo Nippon Sanso) atmosphere was maintained at 2.4×10^{-3} Pa. When the isotope oxygen gas $^{18}O_2$ was supplied to the substrate through a radical gun, two experimental conditions were used to control the oxygen isotope concentration. First, the power to the radio frequency (RF) generator of the radical source was turned off. Then, the radical source RF power (300 W) was turned on to supply radical ^{18}O into the growth chamber. During application of the radical source, we confirmed oxygen radicals from the luminescence spectra from the plasma of the radical source. In addition, ionized oxygen was removed by an electrostatic deflector. The film growth conditions are listed in Table 1.

The crystallinity of the film was characterized using X-ray diffraction (XRD, X'Pert PRO MRD, Philips) with a $K\alpha_1$ monochromator. The crystal structure was identified from 2θ–θ measurements. The degree of orientation was characterized by an Omega scan measurement around the ZnO (0 0 2) diffraction. Surface morphologies were evaluated using atomic force microscopy using a dynamic force mode. The optical properties were characterized by the transmittance and photoluminescence measurements. The transmittance measurement was conducted with a double-beamed spectrometer (JASCO, V-550) with a single monochromator. The photoluminescence spectra were measured by a RPM2000 (ACCENT) with He–Cd laser excitation (Kimmon Electric Co., Ltd., $\lambda = 325$ nm, 0.4 W/mm^2). These optical characterizations were carried out in the range between 350 and 650 nm at room temperature.

Oxygen isotopic concentrations were analyzed by secondary ion mass spectrometry (SIMS) using a double focusing mass spectrometer (SIMS, CAMECA, ims 4f).[22] Cs^+ ions were employed as the primary ion with 10 keV acceleration energy. The primary ion current was maintained at approximately 5 nA. The analyzed scanning area was 125 μm^2. The analyzed secondary ions were the negative ions, $^{16}O^-$ and $^{18}O^-$. In these analysis experiments, the mass resolution power $M/\Delta M$ of the SIMS was maintained above 2000 to eliminate interference of the H_2O mass spectrum. The analyzed crater depths were measured using a contact-mode surface profiler (Dektak3030).

The time dependence of the secondary ion intensities was converted to equivalent depths, assuming that the sputtering rate by the primary ion beam was constant during the SIMS analysis. The error of depth due to this assumption was less than a few %, according to preliminary experimental results. The ^{18}O isotope concentration was obtained from the secondary ion intensities as follows:

$$C_{^{18}O} = \frac{I(^{18}O)}{I(^{16}O) + I(^{16}O)} \quad (1)$$

Table 1
Growth conditions of thin films.

Sample	Laser irradiation frequency (Hz)	Radical condition	Growth rate (nm/s)	Film thickness (nm)	Atmosphere
1	10	OFF	0.17	2500	$^{18}O_2$
2	5	ON	0.05	750	$^{18}O_2$
A	5	OFF	0.04	200	$^{16}O_2$
B	5	ON	0.04	200	$^{16}O_2$
C	5	OFF–ON–OFF	0.04	400	$^{18}O_2$

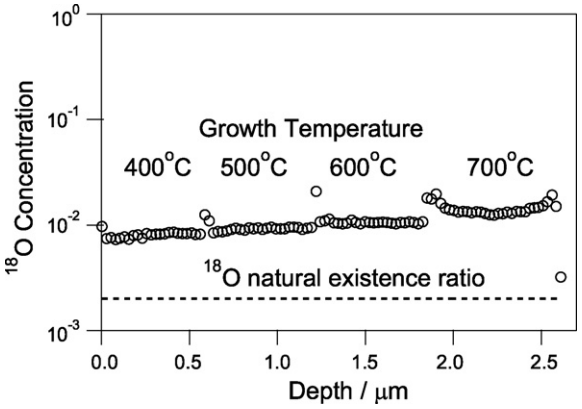

Fig. 1. Depth profile of the substrate temperature dependence of ^{18}O concentration (Sample-1).

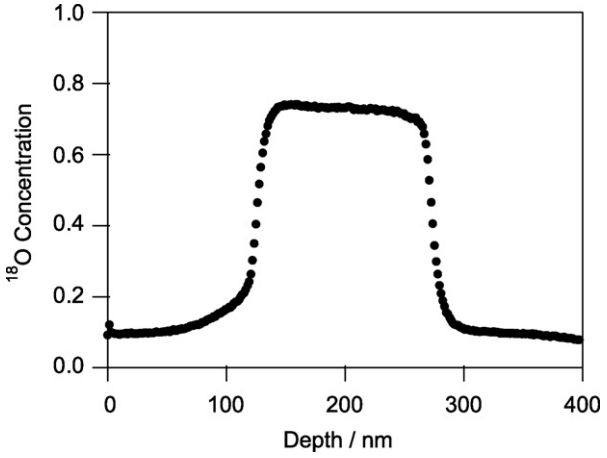

Fig. 3. SIMS depth profile of Sample-C.

3. Results and discussion

Fig. 1 shows the depth profile of the substrate temperature dependence of the ^{18}O concentration for Sample-1. The ^{18}O concentration was approximately 1%. The temperature dependence of the ^{18}O concentration was measured. When the temperature was higher, ^{18}O concentration was also higher. The natural concentration of ^{18}O is approximately 0.2%; therefore approximately 1% of oxygen from the atmosphere was exchanged.

Fig. 2 shows the depth profile of the substrate temperature dependence of the ^{18}O concentration for Sample-2. This film was grown at several substrate temperatures (600, 500, 400, 300 and 200 °C) with ^{18}O radical irradiation. The results show that the ^{18}O concentration was independent of the film growth temperature. This sample contained approximately 75% ^{18}O supplied from the atmosphere as a radical. In addition, the concentration was almost independent of the substrate temperature. If ^{16}O is exchanged for ^{18}O in the plume, it is right that no dependence was observed for the substrate temperature. Meanwhile, if the exchange occurred at the surface of the growing film, then the exchange amount should also be independent of the substrate temperature. These details are discussed further below.

Fig. 3 shows the depth profile of the ^{18}O isotope concentration in Sample-C as analyzed by SIMS. In this figure, the left side of the graph indicates the top of the film and the right side indicates the bottom of the film. The concentration of ^{16}O in natural oxygen was approximately 99.8%, in other words, 99.8% of oxygen in the total oxygen of the target ZnO ceramics was ^{16}O. In this figure, the ^{18}O concentration of the isotopic bottom layer was approximately 10%. This result indicates that 10% of the oxygen from the target ZnO ceramics was exchanged to ^{18}O. In the center layer, in which the isotope radical oxygen, $^{18}O^*$, was supplied during film growth, the ^{18}O concentration was approximately 70%. In the growth term of the ^{18}O-enriched layer, 70% of ^{16}O from the ZnO target ceramics was exchanged for ^{18}O. In the isotopic layer boundary between $Zn^{16}O$ and $Zn^{18}O$, the change in the ^{18}O concentration was sharp; therefore, rapid diffusion of the oxygen did not occur in the period of the film growth.

Fig. 4 shows the XRD patterns of the as-deposited film for Samples-A, B, and C. This figure shows that the films were a single phase of wurtzite-type ZnO and were *c*-axis-oriented because only (0 0 *l*) diffractions were observed. The full-width-at-half-maximum (FWHM) of 2θ for the ω-scan is shown in Table 2. FWHM of 2θ for Sample-C was smaller than for Sample-A or B. This difference was dependent on the film thickness.

Fig. 5 shows AFM images of the surface of the film. In the AFM measurements, Samples-A and B had a grain size of

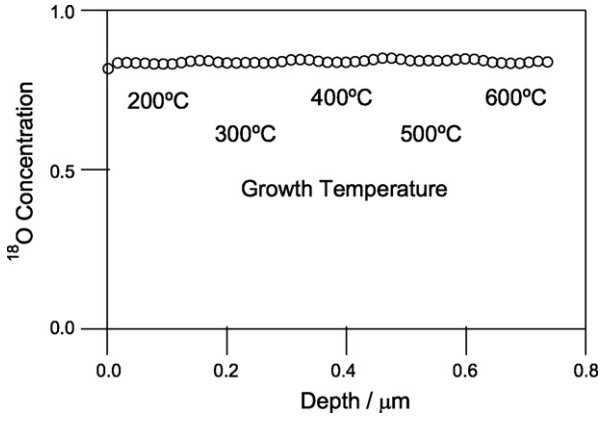

Fig. 2. Depth profile of the substrate temperature dependence of ^{18}O concentration (Sample-2 which was $^{18}O^*$ irradiated growth film).

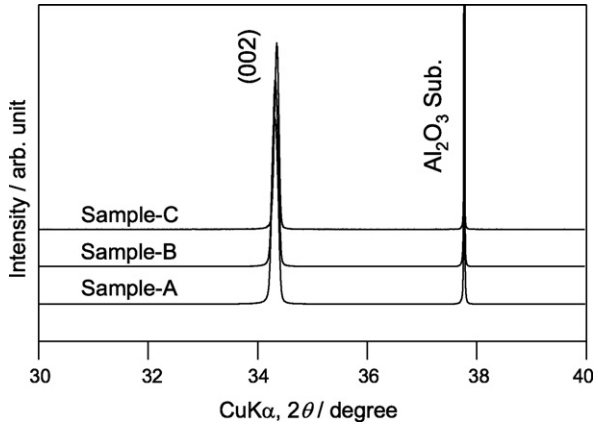

Fig. 4. XRD patterns of Sample-A, B and C.

Table 2
Structural data of the thin films.

Sample	Radical condition	Growth rate (nm/s)	Film thickness (nm)	Arithmetic roughness, R_a (nm)	FWHM of 2θ (°)	FWHM of ω-scan (°)
A	OFF	0.04	200	0.6	0.127	0.27
B	ON	0.04	200	0.4	0.122	0.24
C	OFF–ON–OFF	0.04	400	0.4	0.094	0.21

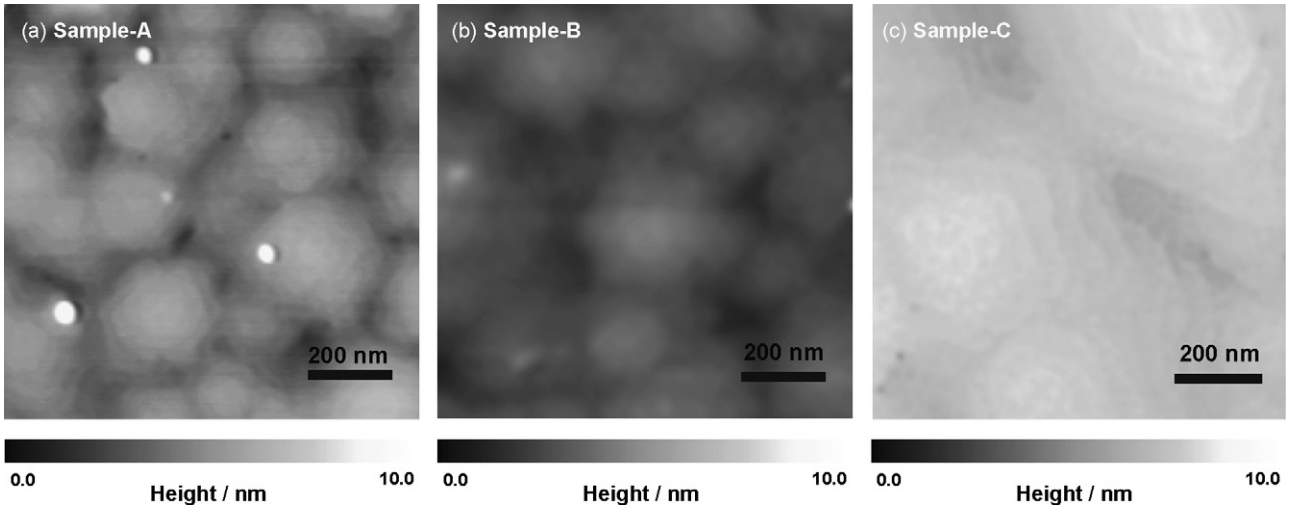

Fig. 5. AFM images of the film surface: (a) grown with O_2, (b) grown with oxygen radical (O^*) irradiation and (c) grown with $^{18}O_2/^{18}O^*/^{18}O_2$.

300 nm, whereas the grain size in Sample-C was approximately 500 nm. The film thickness is believed to be the main factor for controlling the grain size among the samples deposited at the same temperature. All of the AFM images show hexagonal-shaped grains due to the exposure of the *c*-face of the wurtzite structure. The roughness values of the films are also listed in Table 2, which were under 1% of the total thickness. The step shape can be easily seen in the grains and the lattice growth therefore occurred almost layer by layer.

Photoluminescence (PL) and UV–vis transmittance measurements were carried out to characterize the optical properties of Sample-C. Fig. 6 shows the UV–vis transmittance and photoluminescence spectra. From UV–vis transmittance spectra, it is seen that the film was transparent in the visible wavelength regime and absorption at the band edge was sharp. In this measurement, no absorption due to defects in the lattice was observed. In the PL measurement, band-edge luminescence at 375 nm was observed. No broad luminescence spectra in the visible region were seen. This visible luminescence is believed to be caused by point defects in the wurtzite structure.[23]

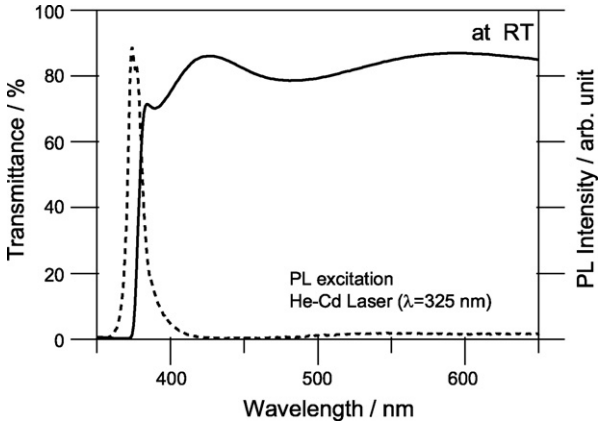

Fig. 6. UV–vis transmittance (solid line) and PL spectrum (dashed line) of Sample-C.

Two different mechanisms can be considered for the formation of ^{18}O-enriched ZnO under the radical irradiation. The first is that the oxygen radical accelerates the exchange reaction between the oxide ion in the solid and radical oxygen at the solid surface. Secondly, the exchange reaction occurs in the laser-ablation plume. In order to clarify the exchange mechanism between the radical oxygen and the lattice oxide ions, the radical oxygen was irradiated onto a ZnO single crystal without laser ablation. If the former mechanism is dominant, the sample surface should be covered with ^{18}O. In the latter case, the exchange ratio should be small, because of the rack of the plume.

The results of SIMS analysis are shown in Fig. 7. It is indisputable from the results that ^{18}O ions were introduced into the lattice. Even if the exchange reaction on the solid surface were to occur, it would seem that the concentration of ^{18}O ions at the surface of a single crystal (approximately 1.4×10^{22} ions/cm^3) would be different from that on the thin films (approximately 3.3×10^{22} ions/cm^3), on which both the laser and radicals were irradiated. Furthermore, ^{18}O ions were found in the interior of the single crystal.

Several reasons can be considered for this discrepancy and behavior. One is a diffusion contribution during radical irradiation. In this case, the ^{18}O concentration should be held in equilibrium with that of the isotope radical of 3.3×10^{22} ions/cm^3. Tomlins et al. reported the oxygen diffusion characteristics in

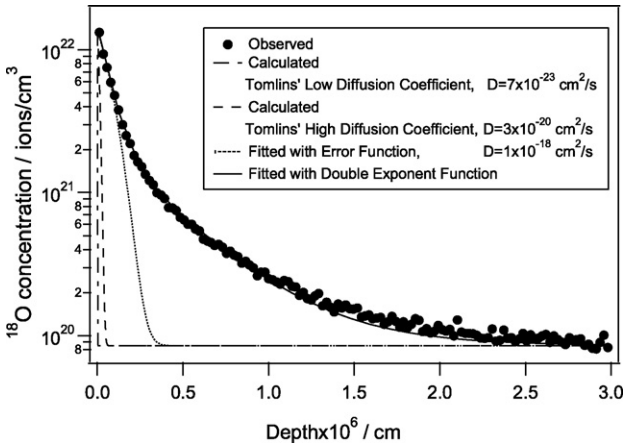

Fig. 7. ^{18}O concentration in the single crystal irradiated by radical oxygen without laser-ablation. Dashed and dashed-dotted line, estimated depth profiles using Tomlins' diffusion data: Ref. [24].

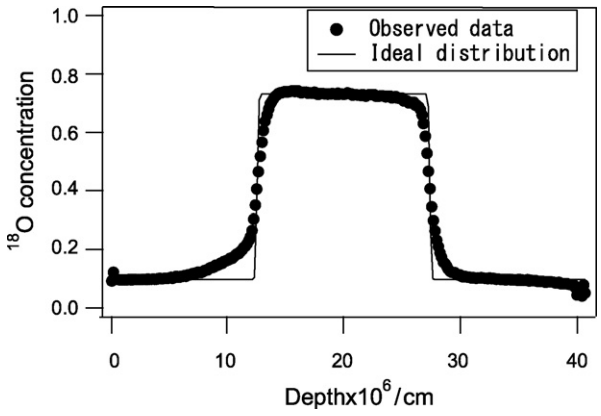

Fig. 8. Comparison between observed ^{18}O distributions and estimated one (Sample-C).

ZnO single crystals.[24] According to their results, the temperature dependence is different for each sample. Two extrapolated diffusion coefficients were calculated at 873 K, the temperature during the radical irradiation. One is 3×10^{-20} cm^2/s, and the other is 7×10^{-23} cm^2/s. The estimated values are plotted in Fig. 7. The dashed line is for 3×10^{-20} cm^2/s of the diffusion coefficient and the dashed-dotted line is for 7×10^{-23} cm^2/s. Neither of these can explain the depth profile. Assuming that this depth profile is due to diffusion, the calculated diffusion coefficient corresponds to 1×10^{-18} cm^2/s, which is much higher than Tomlins' data. It is, therefore, unlikely that the depth profile is caused only by the diffusion contribution. The depth shape is well fitted by two components using an exponential decay function, plotted with a solid line in Fig. 7. This means that the depth profile in the single crystal consists of two contributions.

Although ^{18}O exists only at the surface with a delta function shape, artificial tailing occurs in the SIMS profile primarily as a result of the residual ion mixing effect.[25] In the present analysis condition, the exponential decay length should be 5 nm, almost the same as the experimental decay length of the first component near the surface of approximately 6 nm. The shape of the depth profile near the surface is related to ion mixing by the primary ion beam during analysis. If this contribution is dominant and the isotope exchange reaction progresses sufficiently, the total number of ^{18}O in the solid is almost the same as that of the surface oxygen sites, or more. The estimated value is approximately 1.6×10^{15} ions/cm^2 which is on same order as the theoretical value of 1.09×10^{15} ions/cm^2 but larger. The excess amount of ^{18}O originated from the second exponential component, which is considered to be related to the dislocation pipe diffusion of oxide ions. Thus, it is clear that the enrichment mechanism of the oxygen isotope in laser-ablation is caused by the enhancement of the isotope exchange reaction on the solid surface.

Using the sharpness of the single crystal data, the ideal distribution, including the analytical tails, is plotted in Fig. 8. The observed data indicates a slightly broadened distribution, compared with the ideal distribution. The broadening due to equilibrium diffusion of oxide ions is smaller than the actual data, as mentioned above. Even though the origin of the broadening is not certain, it is considered to be related to oxide ion diffusion through non-equilibrated oxygen defects during the deposition process or the roughness of the sample surface.

4. Conclusions

ZnO thin films were deposited by means of PLD, using an FHG-YAG laser as the light source for the target ablation. Although ^{18}O gas was introduced during the deposition, the ^{18}O concentration remained below a 10% level. By applying radicals of ^{18}O, this value became approximately 70%. This behavior is little dependent on the deposition temperature. Using these conditions, ZnO thin films with isotopic heterostructures were successfully obtained.

The mechanism of oxygen exchange between atmospheric oxygen and oxide ions in the solid, i.e. oxygen radical exchange with solid oxide ions on the sample surface, was clarified using SIMS analysis data of the ^{18}O radical irradiated single crystal without laser ablation. Shape broadening was observed in the heterostructured thin films due to non-equilibrium oxygen diffusion or sample roughness.

Acknowledgements

This work was partially supported by a Grant-in-Aid for Scientific Research (A) (No. 19201019) from the Japan Society for the Promotion of Science and by a research grant from The Murata Science Foundation.

References

1. Ohashi, N., Kataoka, K., Ohgaki, T., Sakaguchi, I., Haneda, H., Kitamura, K. *et al.*, Role of crystalline polarity in interfacial properties of zinc oxide varistors. *Jpn. J. Appl. Phys.*, 2007, **46**, L1042–L1044.
2. Tsukazaki, A., Ohtomo, A., Onuma, T., Ohtani, M., Makino, T., Sumiya, M. *et al.*, Repeated temperature modulation epitaxy for p-type doping and light-emitting diode based on ZnO. *Nat. Mater.*, 2005, **4**, 42–46.
3. Liu, M. and Kim, H. K., Ultraviolet detection with ultrathin ZnO epitaxial films treated with oxygen plasma. *Appl. Phys. Lett.*, 2005, **84**, 173–175.
4. Mitsuyu, T., Ono, S. and Wasa, K., Structure and SAW properties of rf-sputtered single-crystal films of ZnO on sapphire. *J. Appl. Phys.*, 1980, **51**, 2464–2470.

5. Zhu, J., Chen, Y., Saraf, G., Emanetoglu, N. W. and Lu, Y., Voltage tunable surface acoustic wave phase shifter using semiconducting/piezoelectric ZnO dual layers grown on r-Al_2O_3. *Appl. Phys. Lett.*, 2006, **89**, 103513.
6. Shiosaki, T., Fukuda, S., Sakai, K., Kuroda, H. and Kawabata, A., Second harmonic generation in as-sputtered ZnO optical waveguide. *Jpn. J. Appl. Phys.*, 1980, **19**, 2391–2394.
7. Heideman, R. G., Lambeck, P. V. and Gardeniers, J. G. E., High quality ZnO layers with adjustable refractive indices for integrated optics applications. *Opt. Mater.*, 1995, **4**, 741–755.
8. Pfeiffer, L., West, K. W., Stormer, H. L. and Baldwin, K. W., Electron mobilities exceeding 10^7 cm^2/V s in modulation-doped GaAs. *Appl. Phys. Lett.*, 1889, **55**, 1888–1890.
9. Matsuoka, T., Nakazawa, T., Ohya, T., Taniguchi, K., Hamaguchi, C., Kato, H. *et al.*, Zone-folding effect in short-period $(GaAs)_n/(AlAs)_n$ superlattices with n in the range 3–15. *Phys. Rev. B*, 1991, **43**, 11798–11805.
10. Ohta, H., Kim, S., Mune, Y., Mizoguchi, T., Nomura, K., Ohta, S. *et al.*, Giant thermoelectric Seebeck coefficient of two-dimensional electron gas in $SrTiO_3$. *Nat. Mater.*, 2007, **6**, 129–134.
11. Makino, T., Segawa, Y., Kawasaki, M. and Koinuma, H., Optical properties of excitons in ZnO-based quantum well heterostructures. *Semicond. Sci. Technol.*, 2005, **20**, S78–S91.
12. Göbel, A., Ruf, T., Fischer, A., Eberl, K. and Cardona, M., Optical phonons in isotope superlattices of GaAs, GaP, and GaSb studied by Raman scattering. *Phys. Rev. B*, 1991, **59**, 12612–12621.
13. Morita, K., Itoh, K. M., Muto, J., Mizoguchi, K., Usami, N., Shiraki, Y. *et al.*, Growth and characterization of $^{70}Ge_n/^{74}Ge_n$ isotope superlattices. *Thin Solid Films*, 2000, **369**, 405–408.
14. Itoh, M., Wang, R., Inaguma, Y., Yamaguchi, T., Shan, Y.-J. and Nakamura, T., Ferroelectricity induced by oxygen isotope exchange in strontium titanate perovskite. *Phys. Rev. Lett.*, 1999, **82**, 3540–3543.
15. Itoh, M. and Wang, R., Quantum ferroelectricity in $SrTiO_3$ induced by oxygen isotope exchange. *Appl. Phys. Lett.*, 2000, **76**, 221–223.
16. Müller, K. A. and Burkard, H., $SrTiO_3$: an intrinsic quantum paraelectric below 4 K. *Phys. Rev. B*, 1979, **19**, 3593–3602.
17. Tsoi, S., Lu, X., Ramdas, A. K., Alawadhi, H., Grimsditch, M., Cardona, M. *et al.*, Isotopic-mass dependence of the A, B, and C excitonic band gaps in ZnO at low temperatures. *Phys. Rev. B*, 2006, **74**, 165203.
18. Serrano, J., Manjón, F. J., Romero, A. H., Widulle, F., Lauck, R. and Cardona, M., Dispersive phonon linewidths: the E_2 phonons of ZnO. *Phys. Rev. Lett.*, 2003, **90**, 055510.
19. Haneda, H., Ohgaki, T., Sakaguchi, I., Ryoken, H., Ohashi, N. and Yasumori, A., SIMS analysis of impurities and nitrogen isotopes in gallium nitride thin films. *Appl. Surf. Sci.*, 2006, **252**, 7265–7268.
20. Ryoken, H., Ohashi, N., Sakaguchi, I., Adachi, Y., Hishita, S. and Haneda, H., Structures and properties of (Zn,Mg)O films studied from the aspect of phase equilibria. *J. Cryst. Growth*, 2006, **287**, 134–138.
21. Fons, P., Iwata, K., Yamada, A., Matsubara, K. and Niki, S., Uniaxial locked epitaxy of ZnO on the *a*-face of sapphire. *Appl. Phys. Lett.*, 2000, **77**, 1801–1803.
22. Haneda, H., Role of diffusion phenomena in the processing of ceramics. *J. Ceram. Soc. Jpn.*, 2003, **111**, 439–447.
23. Ohashi, N., Ishigaki, T., Okada, N., Sekiguchi, T., Sakaguchi, I. and Haneda, H., Effect of hydrogen doping on ultraviolet emission spectra of various types of ZnO. *Appl. Phys. Lett.*, 2002, **80**, 2869–2871.
24. Tomlins, G. W., Routbort, J. L. and Mason, T. O., Oxygen diffusion in single-crystal zinc oxide. *J. Am. Ceram. Soc.*, 1998, **81**, 869–876.
25. Boulakroune, M., Oualkadi, A., Benatia, D. and Kezai, T., New approach for improvement of secondary ion mass spectrometry profile analysis. *Jpn. J. Appl. Phys.*, 2007, **46**, 7441–7445.